Characterisation of fungal diseases on winter wheat crop using proximal and remote multispectral imaging

R. Bebronne[1], A. Michez[2], V. Leemans[1], P. Vermeulen[3], B. Dumont[4], B. Mercatoris[1]
[1]*Biosystems Dynamics and Exchanges, TERRA Teaching and Research Centre, Gembloux Agro-Bio Tech, Liège University, Passage des Déportés, 2, 5030, Gembloux, Belgium*
[2]*Forest Management, TERRA Teaching and Research Centre, Gembloux Agro-Bio Tech, Liège University, Passage des Déportés, 2, 5030, Gembloux, Belgium*
[3]*Walloon Agricultural Research Centre, Valorisation of Agricultural Products Department, Food and Feed Quality Unit, Chaussée de Namur, 24, 5030, Gembloux, Belgium*
[4]*Plant Sciences, TERRA Teaching and Research Centre, Gembloux Agro-Bio Tech, Liège University, Passage des Déportés, 2, 5030, Gembloux, Belgium*
benoit.mercatoris@uliege.be

Abstract

Winter wheat fungal diseases, responsible for high yield losses, can be assessed by computer vision to increase phenotyping performance. This study aims to compare multispectral imagery based on remote and proximal sensing for disease detection. Wavelength selection was achieved by ANOVA and stepwise regression. Prediction of disease severity was performed by means of an artificial neural network based on proximal sensing data. Septoria tritici blotch (STB) requires proximal measurements, but stripe and brown rusts can be detected from UAVs and from the ground. Prediction results obtained gave R^2 of 0.55 and 0.57 for STB and stripe rust respectively.

Keywords: Wheat, fungal diseases, multispectral, unmanned aerial vehicle sensing, proximal sensing

Introduction

Recent study indicates Belgium is the fifth biggest consumer of phytopharmaceutical products for crop management (Service Public de Wallonie, 2018). The use of pesticides has been reduced by half compared to 1995 but has remained stable since 2010 and shows no sign of further decrease (Fioac de Wallonie, 2018). Pesticides are used to prevent the infection of stripe rust, brown rust and Septoria tritici blotch (STB) which are common diseases of winter wheat caused respectively by *Zymoseptoria tritici*, *Puccinia striiformis* and *Puccinia recondita* (Bodson et al., 2017). The strategy to reduce pesticide application in wheat management relies on (i) the selection and evaluation of varieties resistant to biotic stress and (ii) the spraying regulation depending on the severity of disease infection. Conventional assessment is based on visual or manual observations, but these methods suffer from limited phenotype data sets and bias between assessors. These problems can be resolved by use of automated phenotyping platform which can be exploited both for agronomic trial and production fields (Fiorani and Schurr, 2013).
Developing a phenotyping device for early disease detection and to quantify plant health status for wheat has been reported in the literature by means of spectral imaging which has been identified as a key technology for plant phenotyping (Li et al., 2014). In 2004,

Moshou et al. detected stripe rust in wheat by means of proximal sensing with high success rate, highlighting wavebands centred on 543 nm, 630 nm, 750 nm and 861 nm. By using a spectroradiometer in proximal sensing, Krishna et al. (2014) developed a model able to quantify stripe rust severity in wheat. For STB, Yu et al. (2018) accurately discriminated healthy from infected wheat based on hyperspectral proximal measurements.

Most disease detection studies focus on proximal measurements of reflectance in the field (Bravo et al., 2003; Odilbekov et al., 2018) or in a laboratory (Devadas et al., 2009) but few of them consider aerial spectral measurements for disease detection (Nebiker et al., 2016; Huang et al., 2007) which is more adequate for large-scale area such as production field. Moreover, disease detection studies are generally based on artificial disease inoculation leading to field infection occurrence at early growing stages. A combination of stresses can affect winter wheat simultaneously and belatedly in the growing season, complicating spectrally-based detection efforts.

This study aimed to integrate ground-based and aerial multispectral approaches to characterise the three major fungal diseases affecting winter wheat, i.e. stripe rust, brown rust and STB, under natural conditions. The goal was to select the wavebands which could allow the differentiation between healthy and diseased wheat for the two scales and to investigate their potential for disease severity regression on proximal sensing data.

Materials and methods

Field experiment

The experiments took place in fields dedicated to larger agronomic trials on winter wheat, *Triticum aestivum* L., designed in microcrops (1.8 x 6 m) to study the effects of wheat variety, fungal treatment and sowing date on crop yield. The experiments were monitored during the 2017 growing season by aerial remote sensing and during the 2018 growing season by proximal sensing. Both fields were located in Lonzée, Belgium (50° 32' 58" N and 4° 44' 08" E). In 2017, the approach based on unmanned aerial vehicle (UAV) focused on six varieties (Albert, Anapolis, Edgar, Mentor, Reflection and RGT Reform) sown on October 25 under two types of fungal treatments, i.e. no treatment (0T) and two treatments (2T) on May 10 and May 31. Three replications were studied. The experiment of 2018 involved five varieties (Alcides, Benchmark, Edgar, RGT Reform and Triomph) sown on November 16 under 0T and 2T on May 8 and May 24 with four replications. For each experiment, the varieties were chosen based on their disease sensitivity to allow measurement of different levels of infection.

Disease visual assessment

Severities of STB, stripe rust and brown rust were visually assessed at the leaf level. Rust score is a degree of severity based on the Cobb's modified scale (Peterson et al., 1948). STB severity represents the proportion of the leaf affected by symptoms. Five plants were collected for each microcrop. Disease score for each microcrop was the mean of leaf disease score. In 2017, 2T microcrops were not visually assessed and were considered as healthy (disease severity = 0) due to sufficient application of pesticides.

Aerial sensing acquisition, image treatment and statistical analysis

An octocopter UAV (X frame type) was flown over the 2017 agronomic trial on June 1, June 15 and July 7 at 100 m above ground level (AGL) at a speed of 5 ms^{-1}. The Parrot

Sequoia camera (Parrot SA, Paris, France) covering green (550 nm), red (660 nm), red edge (735 nm) and near infrared (790 nm) wavelengths was mounted on the UAV. The full width at half maximum was 40 nm for red, green, near infrared (NIR) and 10 nm for the red edge. The sensor allowed the computation of true reflectance imagery by means of an upward looking sunshine sensor measuring incident lighting and the use of grey calibration plate before each flight survey. Pix4D suite 3.1 (Pix4D SA, Lausanne, Switzerland) was used to perform a photogrammetric 3D reconstruction of the multispectral imagery using the 'Ag Multispectral' predefined workflow. The images acquired by the multispectral sensor were used to derive orthomosaic reflectance maps (0.1 m ground sampling distance, GSD) in the four wavelengths (green, red, near-infrared and red edge). Five white targets were precisely georeferenced using precision differential GPS (Real Time Kinematic GPS, ± 0.03 m mean XYZ accuracy) in order to ensure geometrical and positioning accuracy of the reflectance maps.
At each date, averaged reflectance values were compared between 0T and 2T microcrops. Mean reflectance comparison was achieved by analysis of variance (ANOVA) carried out for each waveband on each date separately. A Kolmogorov-Smirnov test was applied on the samples to guarantee their normality.

Proximal sensing acquisition, image treatment and disease prediction

A multispectral acquisition prototype acquired images at 1 m above the canopy. The system included a monochromatic 12 bit 1.3 Mpixel camera CMOS BCi5 (C-Cam technologies, Leuven, Belgium) combined with optical filters placed on a motorised wheel to place each filter successively in front of the camera (Figure 1). Eleven wavebands were measured centred from 450 to 950 nm by step of 50 nm and with a bandwidth of 40 or 50 nm. To take into account the variations of illumination, each image was normalised by adapting the integration time of the camera based on the reflectance measured on a silicon white reference placed in the field of view of the camera.

Figure 1: Proximal multispectral acquisition system. On the left, the camera and the motorised filter wheel. On the right, the full platform supporting the acquisition system.

For a scene, 11 images were acquired and overlaid to obtain a single multispectral image on which plant-soil segmentation was performed. Since the image normalisation only considered global illumination, an artificial neural network (ANN) was trained to account for light contrast inside the scene of interest by classifying pixels under shady, sunny or cloudy conditions (Figure 2).

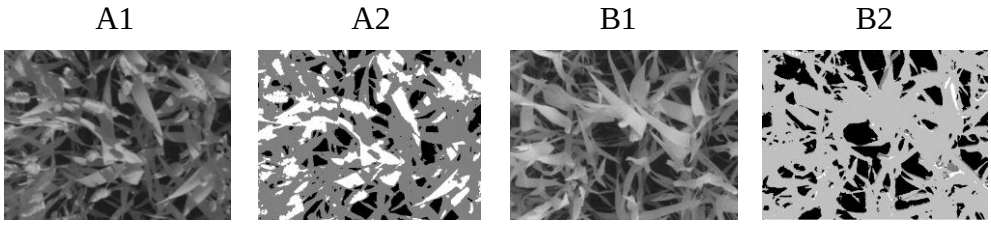

Figure 2: Grey images of winter wheat acquired (A1, B1) and the same images after segmentation (A2, B2) in four classes: soil (black), shady (dark grey), sunny (white), cloudy (light grey)

The mean reflectance was computed for the four groups of plant pixels (mean sunny, mean shady, mean cloudy and mean of total plant pixels). Texture analysis was performed by means of co-occurrence matrix on all plant pixels from which four parameters were extracted: correlation, contrast, energy and homogeneity (Baraldi et Parmigianni, 1995). Considering the 11 layers of a multispectral image, a scene was then characterised by 88 features. A bidirectional stepwise regression was used to establish a model involving the most discriminative features and allowing waveband selection. Based on this feature selection, an ANN was trained and validated using 80% of the dataset and the model was tested on the remaining 20% images. This machine learning method was chosen for its capacity to resolve complex problems and to deal with a small amount of data (Hornik et al., 1989).

Results and discussion

Aerial sensing approach

On June 1, 2017, due to absence of rust on all 0T microcrops except the variety Reflection infected by stripe rust, the other microcrops were only infected by septoria with severities ranging from 4% to 13%. The statistical analysis performed showed no significant mean difference between 0T and 2T (healthy) microcrops (Table 1). STB emerges on the lower leaves (Bahat et al., 1980) which makes it harder to detect from above. Indeed, the aerial nadir perspective induces occlusion on infected leaves below the crop canopy. In order to peek through the canopy and collect unmixed data from lower leaves, the spatial resolution needs to be finer which raises interest for proximal detection of STB.

Table 1: p-values of the mean reflectance difference between infected and healthy microcrops for the three dates and varieties Albert, Anapolis, Edgar, Mentor and RGT Reform. Interaction between variety and health status being significant on July 7 for green waveband, analysis of variance has been split into five for every variety.

p-value	June 1	June 15	July 7
Green	0.24	0.018	[0,045 - 6.95E-07]
Red	0.28	0.033	3.18E-06
Red edge	0.18	0.0002	1.07E-06
Near infrared	0.98	0.0025	4.85E-06

On June 15, all five varieties were healthy regardless of their treatment. The lowest leaves were not taken into account due to their necrosis. However, ANOVA highlighted, by increasing p-value, red edge, NIR, green and red as significant. (Table 1). Even though

STB was absent of the crop, the changes in reflectance values appeared due to accelerated plant senescence originating from previous STB infection. The detection of STB by UAVs is delayed in time.
Between June 15 and July 7, brown rust developed on 0T microcrops up to severities ranging from 76% to 97%. On July 7, differences between 0T and 2T means were more significant than on June 15 for all wavebands (Table 1). This level of significance is probably due to the combination of the damage caused by septoria earlier in the growing season and the strong infection by brown rust. The most significant difference was still observed in the red edge band. However, the red band which showed the least significance on June 15 was the second most significant on July 7 due to symptoms of brown rust characterised by brown to orange spores.
Variety Reflection was reported separately from the other varieties as it was the only variety infected by stripe rust during the acquisition period (31%, 54% and 93% respectively on the three dates of acquisition). It was also infected by septoria but only on June 1 with 21% severity. It was shown that septoria induced no significant mean difference in early infection. However, the ANOVA applied on June 1 highlights NIR (p-value = 0.0014) and red (p-value = 0.0059) as significantly different for the Reflection variety (Table *2*). This difference can be attributed to stripe rust infection. From June 1 to July 7, stripe rust severity kept growing but significance of the red waveband remained stable while the green and red edge bands became increasingly significant. It was hypothesised that stripe rust infection can be detected early due to its yellow/orange spores reflecting light in the red band. Necrosis and cellular structure modifications induced by the fungus lead to changes in NIR (p-value = 7.77E-04) and red edge (p-value = 4.94E-05) bands where differences were the most significant on July 7.

Table 2: p-value of the mean reflectance difference between infected and healthy microcrops for the three dates and variety Reflection only.

p-value	June 1	June 15	July 7
Green	0.094	0.029	0.0077
Red	0.0059	0.0068	0.0054
Red edge	0.23	0.021	4.94E-05
Near infrared	0.0014	0.015	7.77E-04

Proximal sensing approach
An increase in spatial resolution by means of proximal sensing allowed severity regression based on multispectral imagery (**Erreur ! Source du renvoi introuvable.**). Wavelengths of interest (**Erreur ! Source du renvoi introuvable.**) were located in the green (500 and 550 nm) and in the red/red edge (650 and 700 nm) bands. Wavelengths in the NIR band were excluded from the model despite being identified as key wavelengths for septoria detection due to the influence of water in this band (Yu et al., 2018). Prediction tends to underestimate STB severity especially for highly infected microcrops. Images at high severity were acquired on the last acquisition date (June 21) at growth stage 75 (Zadoks et al., 1975) where infected lower leaves were obstructed due to crop density. To improve the regression, shady features could help to detect these lower leaves. However, these features were excluded from the model since at advanced stages almost all the leaves are shaded except the flag leaves. The isolation of infected lower leaves could be assessed by means of sensors measuring depth like stereoscopic systems.

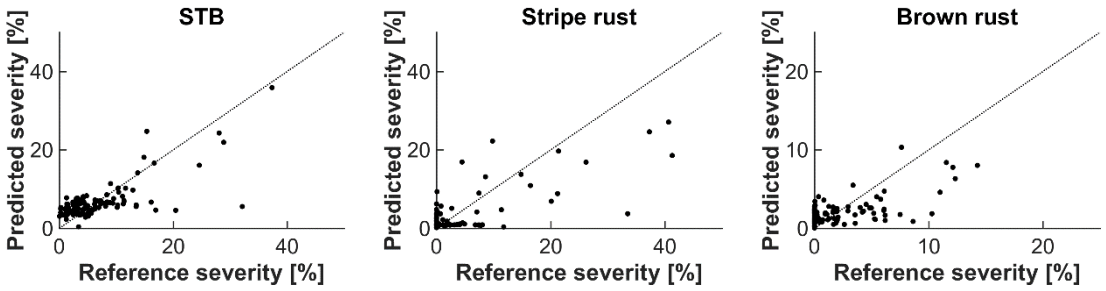

Figure 3: Regression results for STB, stripe rust and brown rust between predicted and measured severity.

These variables are used by the ANN for a regression characterised by a predicted R^2 of 0.55 and a RMSE of 4.35% (**Erreur ! Source du renvoi introuvable.**).
Wavelengths entered in the stepwise model for stripe rust detection in this work cover the spectrum used (Table 3). The waveband centred on 600 nm corresponds to the yellow/orange colour of stripe rust spores. In proximal sensing, Moshou et al. (2004) identified wavebands at 543 ± 10 nm and 861 ± 10 nm as the most discriminating by stepwise regression while Krishna et al. (2014) identified by principal component analysis (PCA) wavelengths at 428 nm and 672 nm. In this study, wavebands centred on 500 nm and 700 nm were the two most discriminative, 850 nm was also highlighted. There seems to be no consensus on proper waveband selection which implies that wavelengths selected are dataset specific. However, it is important to note that stepwise regression and PCA do not include highly correlated variables in the model which is the case for wavebands being close to each other. These variables were used by ANN to give regression results of predicted R^2 of 0.57 and predicted RMSE of 5.37% (Figure 3).
Brown rust detection is assessed mainly based on textural features computed from wavelengths in the NIR and in the red bands (Table 3**Erreur ! Source du renvoi introuvable.**) corresponding respectively to the physiological changes induced by the disease and the colour of the brown rust spores. Reflectance at wavelengths from 550 to 700 nm increased from the first days of inoculation (Kuska et al., 2015). In the literature, Leaf Rust Disease Severity Index 2 (LRDSI2) developed by Ashourloo et al. (2014) reached an accuracy of 86.5% for leaf rust detection and required wavebands centred in 455 nm and 605 nm, which were both part of the model in this work.

Table 3: Features selected by stepwise regression for STB, stripe rust and brown rust detection sorted by increasing order of significance.

STB		**Stripe rust**		**Brown rust**	
Parameters	**λ (nm)**	**Parameters**	**λ (nm)**	**Parameters**	**λ (nm)**
Contrast	700	Energy	700	Correlation	800
Homogeneity	650	Homogeneity	500	Homogeneity	600
Contrast	550	Energy	600	Homogeneity	650
Contrast	500	Mean sunny	850	Homogeneity	450
Energy	650	Mean sunny	900	Energy	800
Mean total	700			Energy	950

Brown rust remained in 2018 at very low severity levels (<13%) which gave results of lower quality with a predicted R^2 of 0.41 and RMSE of 2.40% (Figure 3). This disease should be studied on a highly infected field in order to observe a wider range of infection. The co-development of the two rusts would be very challenging to discriminate.

Conclusions

This study compared multispectral imagery based on remote and proximal sensing for winter wheat fungal disease detection. Regarding STB, the remote approach remains limited to late STB detection. In contrast, proximal sensing improved detection thanks to wavelengths in the red, red edge and green bands. Predictions should be improved in further studies by isolating lower infected leaves. For stripe rust, the stepwise regression model highlighted wavebands in the NIR (850 nm and 900 nm) and in the red (600 nm and 700 nm) which were also retained with significant mean difference for drone-based approach. The coherence of wavelengths between remote and proximal sensing along with the very significant NIR and red mean difference in UAV sensing at 31% severity fosters the potential for stripe rust detection in remote aerial sensing. For brown rust, no specific wavebands of interest were clearly identified by ANOVA in UAV-sensing, making the link between both scales difficult. As for stripe rust, UAV-sensing showed however great potential for brown rust detection and should be tested on wheat infected at lower severity. In proximal sensing, red and NIR were significant but brown rust infection was too low to obtain good regression results.
UAV imagery, due its ability to detect rusts should be used for agricultural management as the larger resolution allows a quick overview of the fields. The data measured at leaf level by proximal sensing could be used in plant phenotyping experimentations to have access to information about STB and to go further than a simple detection for the three diseases. Proximal sensing, by leaf segmentation and texture analysis, displayed a potential for severity prediction of septoria and stripe rust. The results obtained can be used for health status discrimination, but accurate quantification would require an improvement of the multispectral imaging device, especially by setting up a co-registration of the images. Further studies should focus on wavebands of interest identified for each disease with narrower width and should consider more frequent time series measurements to improve detection and quantification.

Acknowledgements

This research has been performed in the framework of PHENWHEAT project financially supported by the Agriculture, Natural Resources and Environment Research Direction of the Public Service of Wallonia, Belgium (Project D31-1385).

References

Ashourloo, D., Mobasheri, M. R., & Huete, A. 2014. Developing two spectral disease indices for detection of wheat leaf rust (Puccinia triticina). Remote Sensing **6** 4723–4740.

Bahat, A., Gelernter, I., Brown, M. B. & Eyal, Z. 1980. Factors affecting the vertical progression of Septoria leaf blotch in short-statured wheats. Phytopathology **70**(3) 179-184.

Baraldi, A. & Parmiggiani, F. 1995. An investigation of the textural characteristics associated with Gray Level Co-occurrence Matrix statistical parameters. IEEE Transactions on Geoscience and Remote Sensing **33**(2) 293–304.

Bodson B., De Proft M. & Watillon B., 2017. Livre Blanc Céréales. Edition février 2017 (White paper cereals. February edition 2017).

Bravo, C., Moshou, D., West, J., McCartney, A., & Ramon, H. 2003. Early disease detection in wheat fields using spectral reflectance. Biosystems Engineering. **84**(2), 137–145.

Devadas, R., Lamb, D. W., Simpfendorfer, S., & Backhouse, D. 2009. Evaluating ten spectral vegetation indices for identifying rust infection in individual wheat leaves. Precision Agriculture **10** 459–470.

Fiorani, F., & Schurr, U. 2013. Future Scenarios for Plant Phenotyping. Annual Review of Plant Biology **64** 267–291.

Hornik K., Stinchcombe M. & White H., 1989. Multilayer feedforward networks are universal approximators. Neural networks **2**(5) 359-366.

Huang, W., Lamb, D. W., Niu, Z., Zhang, Y., Liu, L., & Wang, J. 2007. Identification of yellow rust in wheat using in-situ spectral reflectance measurements and airborne hyperspectral imaging. Precision Agriculture **8**(4-5) 187–197.

Krishna, G., Sahoo, R. N., Pargal, S., Gupta, V. K., Sinha, P., Bhagat, S. et al. 2014. Assessing wheat yellow rust disease through hyperspectral remote sensing. In: International Archives of the Photogrammetry, Remote Sensing and Spatial Information Sciences, Hyderabad, India, **40** 1413-1416

Kuska, M., Wahabzada, M., Leucker, M., Dehne, H. W., Kersting, K., Oerke, E. C. et al. 2015. Hyperspectral phenotyping on the microscopic scale: Towards automated characterization of plant-pathogen interactions. Plant Methods **11(**1) 1-14.

Li, L., Zhang, Q., & Huang, D. 2014. A review of imaging techniques for plant phenotyping. Sensors **14**(11) 20078–20111.

Moshou, D., Bravo, C., West, J., Wahlen, S., McCartney, A., & Ramon, H. 2004. Automatic detection of "yellow rust" in wheat using reflectance measurements and neural networks. Computers and Electronics in Agriculture **44**(3) 173–188.

Nebiker, S., Lack, N., Abächerli, M., & Läderach, S. 2016. Light-weight multispectral uav sensors and their capabilities for predicting grain yield and detecting plant diseases. International Archives of the Photogrammetry, Remote Sensing and Spatial Information Sciences, Pragues, Czech Republic, **41** 963–970.

Odilbekov, F., Armoniené, R., Henriksson, T., & Chawade, A. 2018. Proximal Phenotyping and Machine Learning Methods to Identify Septoria Tritici Blotch Disease Symptoms in Wheat. Frontiers in Plant Science **9**1-11.

Peterson, R. F., Campbell, A. B., & Hannah, A. E. 1948. A diagrammatic scale for estimating rust intensity on leaves and stems of cereals. Canadian Journal of Research **26**(5) 496-500.

Service Public de Wallonie, 2018. Programme wallon de réduction des pesticides 2018-2022 (Walloon program of pesticides reduction 2018-2022). http://diantonio.wallonie.be/files/PWRP_II.pdf. (last accessed 10/08/2018)

Yu, K., Anderegg, J., Mikaberidze, A., Karisto, P., Mascher, F., McDonald, B. A. et al. 2018. Hyperspectral Canopy Sensing of Wheat Septoria Tritici Blotch Disease. Frontiers in Plant Science **9** 1-17.

Zadoks, J. C., Chang, T. T., Konzak, C. F., & Fryer, J. D. 1974. A decimal code for the growth stages of cereals. Weed Research **14** 415–421.